J Mater Sci (2008) 43:7481–7487
DOI 10.1007/s10853-008-2859-8

ULTRAFINE-GRAINED MATERIALS

XRD profile analysis characterization of ultrafine grained Al–Mg alloys

Markus Dinkel · Florian Pyczak · Johannes May · Heinz Werner Höppel · Mathias Göken

Received: 6 March 2008 / Accepted: 2 July 2008 / Published online: 26 July 2008

Abstract The effect of impurities on the crystallite sizes and dislocation densities of ECAP-processed aluminum–magnesium alloys is studied by X-ray diffraction. It is shown that with increasing magnesium content the achievable reduction in crystallite size with ECAP eventually reaches a saturation state and a further reduction of the structural size seems unlikely. Simultaneously the dislocation density increases to a plateau level with increasing Mg content. In annealing experiments the microstructural stability of AlMg0.5 and the resulting changes are investigated by XRD profile analysis. It becomes evident that annealing leads to a moderate increase in crystallite size up to a temperature where accelerated crystallite growth begins. XRD results prior and after fatigue testing show an increase in crystallite size accompanied by a decrease in dislocation density.

Introduction

Ultrafine grained (UFG) materials can exhibit excellent strength and sometimes also ductility [1, 2]. In recent years this and also the promising superplastic forming capabilities [3] have led to an increased interest in research on this class of materials. Several commercial ideas such as the use as hydrogen storage for fuel cells are discussed. UFG materials are already in use as sputtering targets [4] by Honeywell Electronic Materials.

Although there is vast information on the initial structure and the properties of such materials [5], rather little information is found in literature on the effect of alloying elements on the microstructure. Therefore, in the present investigation results gathered from X-ray diffraction measurements will be presented and discussed.

Evaluation of the XRD profiles

Real materials possess different constraints, which alter the shape of a diffracted X-ray beam. Accordingly, the line profile of the material contains valuable information about the material itself.

The evaluation of such XRD-profiles was performed according to the MWP-fit procedure developed by Ribárik and Ungár [6, 7]. In this procedure theoretical profiles for each peak are calculated via ab initio, i.e. physically based, methods and subsequently fitted to the measured profiles. This is done simultaneously for all recorded profiles.

The physical background and equations upon which these calculations are based will be presented shortly. For the complete treatment the reader is referred to the original work [6–9].

Based on the principal deductions and considerations from [9] the following brief description of the process can be given:

For the evaluation of profiles it is assumed that the physical profile of a Bragg reflection is convoluted from

M. Dinkel (✉) · H. W. Höppel · M. Göken
Department of Materials Science and Engineering, Institute 1: General Materials Properties, University Erlangen, Nürnberg, Martensstrasse 5, 91058 Erlangen, Germany
e-mail: markus.dinkel@ww.uni-erlangen.de

Present Address:
F. Pyczak
Institute for Materials Research, GKSS Research Centre Geesthacht, 21502 Geesthacht, Germany

Present Address:
J. May
AREVA NP GmbH, 91052 Erlangen, Germany

two profiles, one representing the size of the crystallites (superscript S) and the other representing the state of distortion of the material (superscript D)

$$I^{\mathrm{p}} = I^{\mathrm{S}} \cdot I^{\mathrm{D}} \tag{1}$$

For ease of calculation the Fourier transform is used

$$A(L) = A^{\mathrm{S}}(L) \cdot A^{\mathrm{D}}(L), \tag{2}$$

where $A(L)$ are the absolute values of the Fourier coefficients of the physical profiles. Here L is the Fourier variable.

Under the assumption that lattice distortions within the crystal are only caused by dislocations, the Fourier coefficient of the strain profile can be expressed as:

$$A_{\mathrm{g}}^{\mathrm{D}}(L) = \exp\left[-\frac{b^2\pi}{2} g^2 L^2 \rho \overline{C} f(L/R_{\mathrm{e}})\right] \tag{3}$$

Here b is the Burgers vector and R_{e} the effective outer cut-off radius of dislocations as derived by Wilkens. $\overline{C}$ is the average dislocation contrast factor, which is a function of the Miller indexes and the elastic constants of the material.

The contribution to the size induced profile broadening is described as follows:

The crystallite size function in powder or bulk nanocrystalline materials can be described as log normal.

$$f(x) = \frac{1}{\sqrt{2\pi}\sigma}\frac{1}{x}\exp\left\{-\frac{[\ln(x/m)]^2}{2\sigma^2}\right\} \tag{4}$$

with m being the median and σ^2 the variance of the size distribution function. Here x is the crystallite size.

Under the assumption of spherical crystallites with this log normal size distribution, the Fourier transform of the size depending part of the profile can then be expressed as

$$\begin{aligned} A^{\mathrm{S}}(L) \sim & \frac{m^3 \exp(4.5\sigma^2)}{3}\operatorname{erfc}\left[\frac{\ln(|L|/m)}{\sqrt{2}\sigma} - 1.5\sqrt{2}\sigma\right] \\ & - \frac{m^2 \exp(2\sigma^2)}{2}\operatorname{erfc}\left[\frac{\ln(|L|/m)}{\sqrt{2}\sigma} - \sqrt{2}\sigma\right] \\ & + \frac{|L|^3}{6}\operatorname{erfc}\left[\frac{\ln(|L|/m)}{\sqrt{2}\sigma}\right] \end{aligned} \tag{5}$$

where erfc is the complementary Gaussian error function.

For clarity, a volume weighted mean crystallite size [6] will be used.

$$\langle x \rangle_{\mathrm{Vol}} = m \exp\left[3.5\sigma^2\right] \tag{6}$$

These procedures have been implemented into the earlier mentioned MWP-fit software.

It is very important to mention that even the volume averaged crystallite sizes are in some discrepancy with grain sizes measured by transmission electron microscopy. This is due to the fact that the XRD profile analysis-measurements are sensitive to very low misorientation differences, which could stem from dislocation cells, walls or even dipoles. Generally, the method is sensitive for coherently scattering volumes or domains. Therefore a direct comparison is not feasible. On the other hand, this can also be regarded as a big advantage as one gets more in-depth information.

Experimental

The investigated series of AlMg-alloys (AlMg0.5, AlMg1, AlMg1.5, and AlMg2, composition data in wt.%) were alloyed and cast at the Department of Physical Metallurgy and Metal Physics at the RWTH Aachen. In addition, samples with commercial purity Al99.5 (CP Al) were included in the investigation. In order to obtain an ultrafine grained microstructure all specimens were subjected to a so-called Equal Channel Angular Pressing (ECAP) process, see [1, 2] for details of the ECAP process. All samples were deformed in a die with a round channel of 12 mm diameter and a channel intersection angle of 90°. The deformation route applied was either route A, i.e. no rotation after the passes, or route B_C, i.e. a 90° rotation was applied after every pass, according to the nomenclature given in [10]. The materials and states investigated are shown in Table 1.

Transmission electron microscopy was performed in a Philips CM 200.

Samples for XRD-measurements were cut, ground, and polished with SiC paper. Final polishing was performed with 1 μm diamond slurry. The XRD profile analysis-measurements were carried out at a double crystal diffractometer, which is equipped with a position sensitive detector, Type Braun OED-50. The setup is schematically shown in Fig. 1. According to Wilkens and Eckert [11] this setup leads to a negligible instrumental broadening of the X-ray diffraction profiles. In general, up to six reflections were measured, starting from the (111) up to the (400) reflection of the material. Acquisition time for the profiles varied for each reflection, but was in the range of 30 min for the (111)-reflections and in excess of 12 h for the (400)-reflections.

Table 1 Investigated materials and states

Materials	Route		No. of passes			Temperature
	A	B_C	4	8	12	
CP Al	–	x	–	x	–	RT
AlMg0.5	x	x	x	x	x	RT
AlMg1	–	x	–	x	–	RT
AlMg1.5	–	x		x		RT-220 °C
AlMg2	x	x	x	x	x	RT

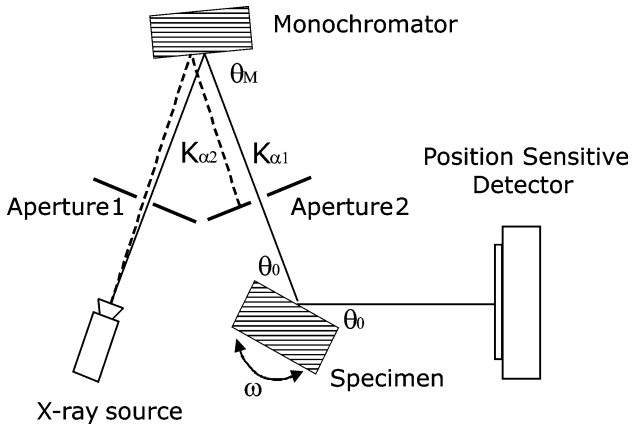

Fig. 1 Schematic image of the double crystal diffractometer used in this study

A very important issue for ultrafine grained material is the question of the thermal stability of the microstructure. Therefore annealing experiments were carried out at various temperatures (100, 125, 155, 190, and 220 °C) on AlMg1.5 specimens and the microstructure was subsequently characterized with XRD.

Fatigued samples were taken out of the gauge length of the fatigue specimens close to the fatigue crack. Fatigue testing was performed in a total strain controlled symmetric push–pull ($R = -1$) test with a total strain amplitude of $\Delta\varepsilon_{tot}/2 = 4.55 \times 10^{-3}$ and a strain rate of $\delta\varepsilon/\delta t = 2 \times 10^{-3}\ s^{-1}$ until failure of the samples. Two samples of AlMg1.5 were measured which were produced by ECAP with eight passes of route A and B_C, respectively.

Results and discussion

Transmission electron microscopy (TEM)

As examples of the typical microstructure found in specimens after the ECAP process, TEM images are shown for AlMg0.5 and AlMg2 in Fig. 2a and b [12]. It can be seen that the grain size is below one micrometer in average. The microstructure of AlMg2 shows a higher amount of dislocations present in the grain interior compared with AlMg0.5. Also it seems that the grain size of AlMg2 is somewhat smaller than that for AlMg0.5. No secondary phases or precipitations can be observed in the microstructure.

X-ray diffraction results

Alloying influence

The influence of magnesium on the crystallite size and the dislocation density is shown in Fig. 3. All samples have been processed by 8 ECAP passes of route B_C. A clear dependency on the Mg content in the alloys is visible. With increasing magnesium content the crystallite size is reduced from about 200 nm for CP Al and AlMg0.5 down to 125 nm for the alloy with the highest Mg concentration, AlMg2. Furthermore, the dislocation density shows a

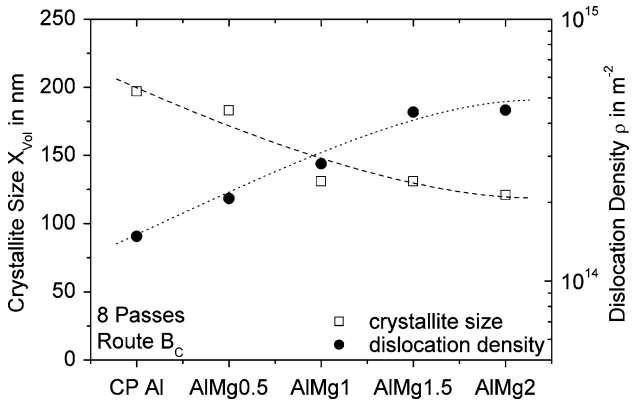

Fig. 3 XRD results of the various alloys depending on the magnesium concentration. All samples were produced by applying 8 ECAP passes using route B_C

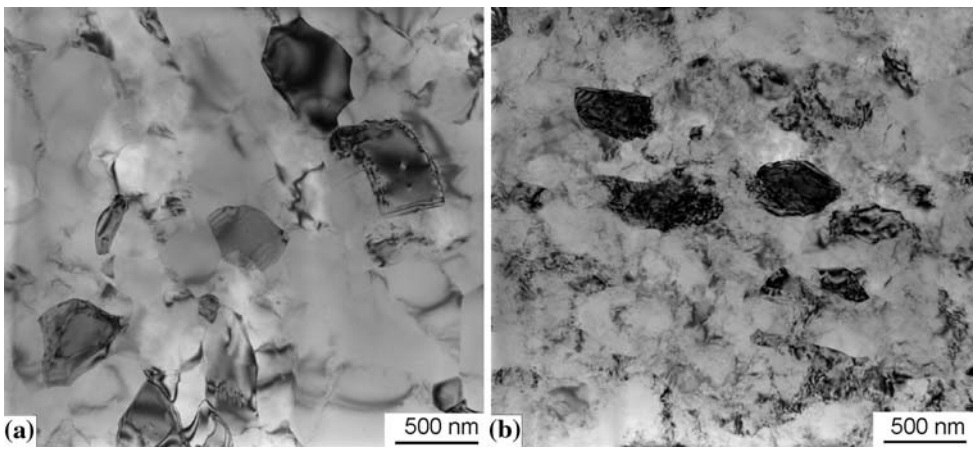

Fig. 2 TEM microstructures of AlMg0.5 (**a**) and AlMg2 (**b**) from [12]

somewhat opposite trend. The amount of dislocations stored in the material rises with increasing Mg content. The dislocation density increases from 1.5×10^{14} m^{-2} for CP Al and AlMg0.5 to about 4.5×10^{14} m^{-2} for AlMg2. The smooth decrease in crystallite size and the increasing dislocation density justifies the assumption that this is purely an alloying effect. The solubility of magnesium in aluminum is significantly higher than 2 wt.%. Therefore the amount of soluted magnesium is four times higher in AlMg2 than in AlMg0.5. The discrepancy between the rather low difference in grain sizes visible in Fig. 2 and the more pronounced difference in the measured XRD-crystallite sizes can be explained as follows. As mentioned before, the crystallite size measurement by XRD profile analysis is rather sensitive to the effect of misorientation between neighboring volumes. This misorientation can be attributed to dislocations, dislocation dipoles, dislocation walls and cells, subgrains, and of course high angle grain boundaries (HAGB) [9]. In the case of a highly distorted microstructure, as in ECAP processed materials, the mobility of dislocations and grain boundaries is very important. At the same time the amount of solute atoms influences this mobility to a great extent. It is obvious that depending on the atomic species the effect on the mobility of dislocation, i.e. the solute drag, and on the grain boundaries, i.e. grain boundary pinning, can be different. A strong solute drag would lead to a decrease in the velocity and mobility of dislocations. Such a decrease would result in a reduction of annihilation effects and therefore a higher dislocation density. This can be seen as the alloys with the higher content of soluted Mg-atoms also show an increase in dislocation density. The smaller crystallite size will be an effect of the reduced annihilation processes as the UFG structure forms from dislocation walls/subgrain structures. These subgrains/walls evolve to HAGBs as a consequence of the repeated shearing.

In the case of commercially pure aluminum the main side element is silicon with 0.34% and a smaller amount of iron (0.19%) [13], whereas in AlMg0.5 the main alloying element is magnesium. It has to be noted that in the case of CP aluminum the side elements mainly form intermetallic phases and are not in solution.

Nevertheless, the total amount of side elements is in the same range as in AlMg0.5, but a difference in the crystallite size and even more in the dislocation density is found. The difference despite a similar content of side elements in CP aluminum and AlMg0.5 is due to the fact that they form small intermetallic phases in the former while being fully soluted in the latter. Furthermore, from the comparison of Figs. 2 and 3 it becomes evident that the crystallite size measured in XRD profile analysis in such strongly plastically deformed materials is mainly determined by dislocation structures and not by high angle grain boundaries. Thus, the increase in magnesium content will enhance the effect on the dislocation mobility and the dislocation density will rise. Additionally, this will lead to a refinement of the coherently scattering domains.

Influence of number of ECAP passes

Figure 4 shows the dependency of the crystallite size and dislocation density on the number of ECAP passes. In this case route B_C was applied and the measurements were only done for AlMg0.5 and AlMg2.

For AlMg2 the crystallite size decreases with an increment in passes from 4 to 8 from about 160 to 120 nm. The application of another 4 passes does not lead to a further refinement of the microstructure and the crystallite size remains at about 120–130 nm. For AlMg0.5 the crystallite size also decreases from 4 to 8 passes (230–180 nm), but increases at 12 passes, where the crystallites size is slightly higher than for 4 passes ($\sim$240 nm).

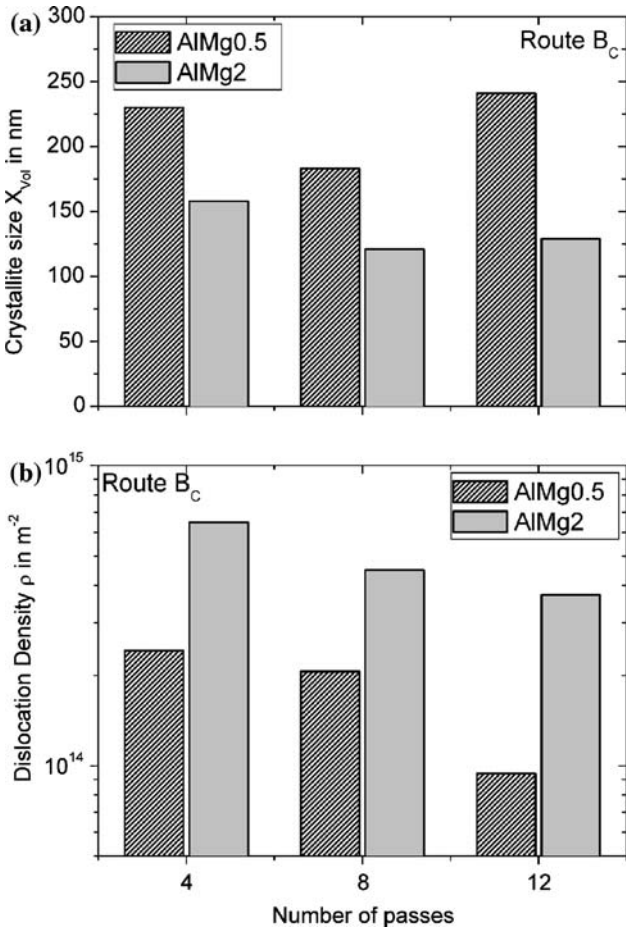

Fig. 4 XRD-measurements of specimens subjected to ECAP using route B_C. Evolution of (**a**) the crystallite size and (**b**) the dislocation density for AlMg0.5 and AlMg2 with varying number of passes

The dislocation density however shows a steady decrease with increasing number of passes for both alloys. For AlMg2 the dislocation density is at $\sim 5 \times 10^{14}$ m^{-2} after 4 passes and drops to $\sim 3 \times 10^{14}$ m^{-2} after 12 passes. For the lower alloyed AlMg0.5, this reduction is comparable with the dislocation density of 1.5×10^{14} m^{-2} at 4 passes which decreases down to 9×10^{13} m^{-2} after 12 passes.

The evolution of the crystallite size with increasing number of ECAP passes does not follow a general trend, for AlMg0.5 and AlMg2. While for AlMg2 the refinement reaches a saturation state after 8 passes and remains almost constant with four additional ECAP passes, the microstructure coarsens for AlMg0.5. Besides, the dislocation density decreases for both materials with increasing number of passes.

The role and importance of the species and amount of alloying elements was discussed above. In this context the results obtained here can also be explained: Depending on the amount of solved magnesium the mobility of dislocations and thus the dislocation interaction changes. A high amount of magnesium will lead to a stronger interaction and therefore less mobility. It is assumed that most boundaries between coherently scattering volumes are built by dislocation dipoles/walls. This has a direct consequence on the behavior of the material. With an increasing number of passes the size of these domains get reduced until the stage when the distances, i.e. the sizes, in between the boundaries of such volumes are small enough that even the impaired dislocations can move from one side to the other within a pass and annihilate in the boundary. Most likely there is no change in the microstructure after the eighth pass. Nevertheless, hardness measurements have shown that with increasing number of passes the hardness still increases, see Fig. 5. This hardness increase is assumed to be a result of the increase in misorientation of cell boundaries.

The reduction in dislocation density follows the same trend, as the amount of dislocations in the crystallite interior gets reduced with decreasing crystallite size. As the crystallite size becomes smaller the dislocations can much more easily react with dislocations stored at the grain boundary. Hence, annihilation processes take place at the grain boundaries and the dislocation density is reduced and the misorientation in the material increases accordingly.

Thermal stability

A very important aspect of the applicability of UFG materials is their long-term thermal stability. Therefore annealing experiments have been carried out up to a temperature of 220 °C. It has to be noted that all specimens were taken out of the same ECAP rod. The evolution of the crystallite size and the dislocation density with respect to the annealing temperature is shown in Fig. 6. The crystallite size shows rather moderate growth from initially 140 to $\sim$200 nm at a temperature of 190 °C. Beyond a temperature of 220 °C, the crystallite size increases strongly.

The evolution of the dislocation density resembles this behavior, with a pronounced decrease in density at 150 °C. The data point at 120 °C is rather high, which must be attributed to experimental scatter. The lack of a data point for the dislocation density at 220 °C is due to the resolution limit of the XRD profile analysis method. In such an annealed and therefore recovered state, the dislocation density is below the detection limit. Nevertheless, it is obvious that the onset of recovery processes starts earlier than the onset of crystallite growth. This difference in the behavior is a consequence of the thermal activation. It should be pointed out that the decrease in dislocation density occurs mainly at the expense of free dislocations

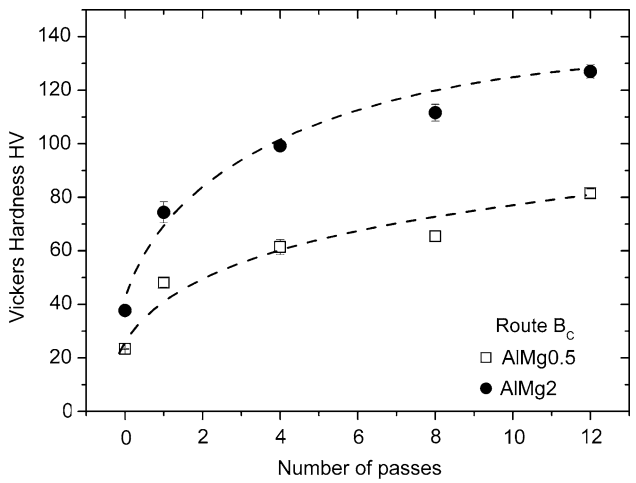

Fig. 5 Hardness evolution with number of ECAP route B_C passes for AlMg0.5 and AlMg2

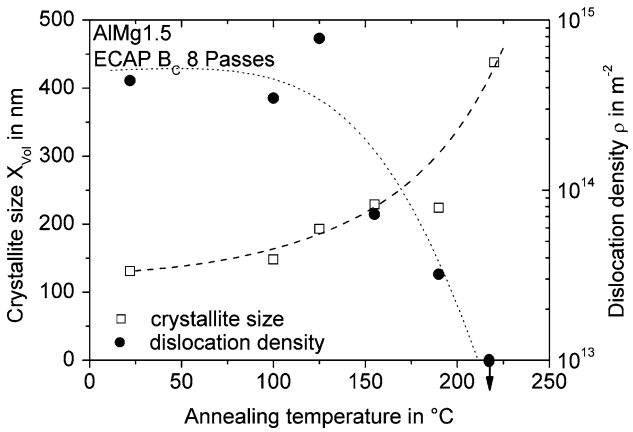

Fig. 6 XRD results of AlMg1.5. Specimens were produced via 8 ECAP passes route B_C

stored in the crystallite interior, i.e. dislocations which are bound in a stable configuration with other dislocations will remain in the material. By thermal activation the movement of these dislocations is easier and therefore annihilation is more likely to occur. This can also lead to a moderate increase in the measured crystallite size, which can be observed simultaneously, because, as mentioned before, even dislocation dipoles might attribute to the size dependent broadening. At higher temperatures, the cooperative movement of—at room temperature stable—dislocation networks and configurations is enabled, and this will lead to the observed pronounced crystallite growth. Furthermore, the movement of high angle and low angle grain boundaries will lead to annihilation of dislocations, and therefore the overall dislocation density in the material will decrease further.

Influence of cyclic deformation on the microstructure

Total strain controlled fatigue experiments have been carried out to evaluate the effects of alloying and the potential of such ultrafine grained materials in terms of cyclic strength. The evolution of the crystallite size and dislocation density prior and after fatigue loading is shown in Fig. 7. Here the dislocation density and crystallite size are plotted for two different samples of AlMg0.5, which were prepared by routes A and B_C, respectively.

For the specimen of route B_C a fatigue life of 3,500 cycles to failure (N_f) is found, which is significantly smaller than for route A ($N_f = 5{,}000$) [12]. Also the latter shows a higher stress amplitude with $\Delta\sigma/2 \approx 280$ MPa compared to $\Delta\sigma/2 \approx 255$ MPa for Route B_C.

Prior to fatigue testing, the crystallite size of both samples route A and B_C is similar and the dislocation density differs only slightly. After fatigue testing, a clear difference is found. The shorter fatigue life of the route B_C sample is accompanied by a more pronounced increase in the crystallite size than for route A. From the initial crystallite size (X_{Vol}) of approximately 130 nm for both routes, the size increased to 250 nm for the route B_C sample and 220 nm for the route A sample. The dislocation density resembles an opposite behavior with a stronger decrease observable for the route B_C sample. For this sample a drop of the dislocations density from initially 4.4×10^{14} to 1.7×10^{14} m^{-2} is found, whereas for the route A sample the dislocation density decreases from 5.0×10^{14} to 2.4×10^{14} m^{-2}.

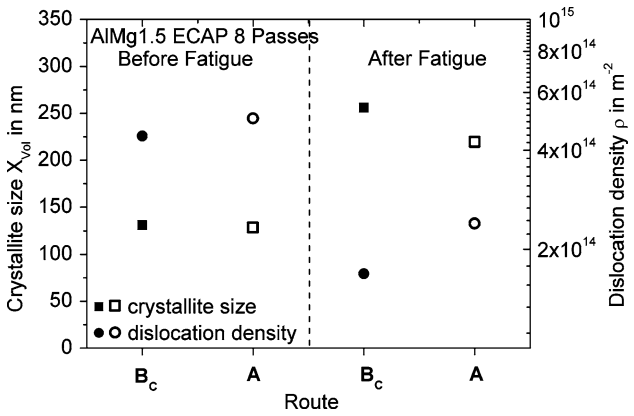

Fig. 7 XRD results of AlMg1.5: Specimens were produced via 8 Passes either route A or B_C. Fatigue samples were tested with a total strain amplitude of $\Delta\varepsilon_{tot} = 4.55 \times 10^{-3}$ and a strain rate of $\delta\varepsilon/\delta t = 2 \times 10^{-3}$ s^{-1}

In the context of the higher stress amplitude for route A these results do seem meaningful, because a higher dislocation density and a finer crystallite size would result in a higher strength of the material at a given total strain amplitude.

The change in microstructure due to the fatigue testing can be described as follows. From the cyclic deformation curve [14] an initial softening of both materials can be seen. This can be attributed to spontaneous annihilation processes which are a result of the plastic strain during fatigue testing. In materials with conventional grain sizes, quasi-stable structures like cell or vain structures or persistent slip bands evolve as a result of cyclic plastic deformation. In the case of ultrafine grained materials such structures would be larger than the crystallite sizes. Due to the reduced crystallite boundary mobility, attributed to the pinning of the boundaries by magnesium, an enhanced crystallite growth cannot take place; thus, the increase in crystallite size is most likely attributed to the dissolving of dipole and ECAP induced cell structures, which will lead to the apparent growth of the crystallite size. The decrease in dislocation density is a consequence of the already-mentioned initial spontaneous annihilation processes and the dissolving of dipoles. As indicated by the pronounced cyclic stability a dynamic equilibrium of dislocation formation and recovery evolves.

The difference in the behavior between route A and route B_C samples can be explained by texture effects. Route A samples generally exhibit a ⟨110⟩-texture whereas route B_C samples are ⟨111⟩ textured [14]. In aluminum, the (111) direction is elastically stiffer than the (110) direction. In a total strain controlled fatigue test, this leads to higher plastic strains for the route B_C sample compared to the route A sample, which results in the higher fatigue life for route A and leads to more recovery in route B_C.

Conclusions

With the method of XRD-line profile analysis the crystallite and dislocation microstructure of ultrafine grained

materials can be investigated quantitatively in an efficient way and with a very high resolution. Furthermore, a much larger material volume is examined compared to TEM measurements. The results obtained on different states of UFG Al and UFG AlMg can be summarized as follows:

- The crystallite refinement of AlMg alloys with ECAP processing is strongly dependent on the concentration and the type of the alloying elements.
- An increase in the number of ECAP passes does not necessarily lead to a finer microstructure. Rather a saturation state is reached accompanied by a decrease in the dislocation density. This might be accompanied by an increase in the portion of high angle boundaries.
- Thermal recovery of the dislocation structure takes place even before the onset of a pronounced crystallite growth.
- Total strain controlled fatigue testing of ultrafine grained materials leads to an increase of the crystallite size and a decrease of dislocation density. This happens due to spontaneous annihilation of dislocations and the dissolving of dipoles and dislocation walls during deformation.

Acknowledgement We are grateful for the help, assistance and tutorial of Prof. Dr. T. Ungár concerning the MWP-fit method.

References

1. Valiev RZ, Ishlamagaliev RK, Alexandrov IV (2000) Prog Mater Sci 45:103. doi:10.1016/S0079-6425(99)00007-9
2. Valiev RZ, Estrin Y, Horita Z, Langdon TG, Zehetbauer MJ, Zhu YT (2006) JOM 58(4):33. doi:10.1007/s11837-006-0213-7
3. Xu C, Furukawa M, Horita Z, Langdon TG (2003) Adv Eng Mater 5(5):359. doi:10.1002/adem.200310075
4. Honeywell Electronic Materials, http://www.honeywell.com
5. Ribárik G, Ungár T, Gubicza J (2001) J Appl Cryst 34:669. doi:10.1107/S0021889801011451
6. Ungár T, Gubicza J, Ribárik G, Borbély A (2001) J Appl Cryst 34:298–310. doi:10.1107/S0021889801003715
7. Wilkens M (1970) Phys Status Solidi (a) 2:359. doi:10.1002/pssa.19700020224
8. Langford JI, Louer D, Scardi P (2000) J Appl Cryst 33:964. doi:10.1107/S002188980000460X
9. Gubicza J, Ribárik G, Bakonyi I, Ungár T (2001) J Nanosci Nanotechnol 1(3):343. doi:10.1166/jnn.2001.039
10. Furukawa M, Iwahashi Y, Horita Z, Nemoto M, Langdon TG (1998) Mater Sci Eng A 257:328. doi:10.1016/S0921-5093(98)00750-3
11. Wilkens M, Eckert K (1964) Z Naturforschg 19a:459
12. May J, Dinkel MK, Amberger D, Höppel HW, Göken M (2007) Metal Mater Trans A 38A:1941. doi:10.1007/s11661-007-9110-0
13. May J, Höppel HW, Göken M (2004) Scr Mater 53:189. doi:10.1016/j.scriptamat.2005.03.043
14. Höppel HW, May J, Göken M (2008) In: 6th International Conference on Low Cycle Fatigue. DVM, Berlin; accepted for publication